Structure–performance correlations in the hybrid oxide-supported copper–zinc SAPO-34 catalysts for direct synthesis of dimethyl ether from CO2

Sara Navarro-Jaén, Mirella Virginie, Joëlle Thuriot-Roukos, Robert Wojcieszak, Andrei Khodakov

▶ **To cite this version:**

Sara Navarro-Jaén, Mirella Virginie, Joëlle Thuriot-Roukos, Robert Wojcieszak, Andrei Khodakov. Structure–performance correlations in the hybrid oxide-supported copper–zinc SAPO-34 catalysts for direct synthesis of dimethyl ether from CO2. Journal of Materials Science, 2022, 57 (5), pp.3268-3279. 10.1007/s10853-022-06890-w . hal-03863304

HAL Id: hal-03863304
https://cnrs.hal.science/hal-03863304v1

Submitted on 25 Nov 2022

HAL is a multi-disciplinary open access archive for the deposit and dissemination of scientific research documents, whether they are published or not. The documents may come from teaching and research institutions in France or abroad, or from public or private research centers.

L'archive ouverte pluridisciplinaire **HAL**, est destinée au dépôt et à la diffusion de documents scientifiques de niveau recherche, publiés ou non, émanant des établissements d'enseignement et de recherche français ou étrangers, des laboratoires publics ou privés.

January 2nd, 2022

Structure-performance correlations in the hybrid oxide-supported copper-zinc SAPO-34 catalysts for direct synthesis of dimethyl ether from CO_2

*Sara Navarro-Jaén, Mirella Virginie, Joëlle Thuriot-Roukos, Robert Wojcieszak and Andrei Y. Khodakov**

Univ. Lille, CNRS, Centrale Lille, Univ. Artois, UMR 8181 – UCCS – Unité de Catalyse et Chimie du Solide, F-59000 Lille, France

*corresponding author (andrei.khodakov@univ-lille.fr)

Compliance with Ethical Standards: Yes

Conflict of Interest: The authors declare that they have no conflict of interest.

Abstract

Growing CO_2 emissions lead to global warming, which is currently one of the most challenging environmental phenomena. Direct catalytic hydrogenation to dimethyl ether over hybrid catalysts enables CO_2 utilization, hydrogen and energy storage and produces sustainable fuels and an important platform molecule.

In this paper, we evaluated structure -performance correlations in the bifunctional hybrid copper-zinc SAPO-34 catalysts for direct synthesis of dimethyl ether via CO_2 prepared using zirconia, alumina and ceria used as oxide carriers. Higher copper dispersion and higher CO_2 conversion rate were uncovered over the alumina and zirconia supported catalysts followed by ceria supported counterpart. The CO_2 hydrogenation seems to be principally favored by higher copper dispersion and to a lesser extent depends on the concentration of Bronsted acid sites in the studied catalysts. Because of lower reverse water gas-shift activity, the alumina supported catalysts exhibited a higher dimethyl ether yield compared to the zirconia and ceria supported counterparts.

Keywords: hybrid catalysts; metal dispersion; acidity; CO_2 mitigation; dimethyl ether

1. Introduction

Global warming is currently one of the most important environmental phenomena and has been attributed to the emission of CO_2 from human activities [1–3]. One of the major challenges is to mitigate CO_2 emission by developing sustainable technologies for CO_2 utilization. The catalytic hydrogenation to dimethyl ether (DME) [3, 4] enables the CO_2 utilization, hydrogen and energy storage and manufactures fuels and a platform molecule for chemical industry. To make the CO_2 hydrogeneration sustainable, hydrogen for this reaction should be produced without additional emission of CO_2. DME is one of the most promising environmentally optimized alternatives [5, 6] to the conventional fossil fuels due to its high cetane index (> 55), low emission of CO, NO_x and particulates. Currently, DME is manufactured [7] by methanol dehydration or directly via hydrogenation from syngas (mixtures of carbon monoxide and hydrogen). Major efforts have addressed the DME synthesis from CO_2. Currently, there are two strategies for the production of DME from carbon dioxide [8, 9]: (i) two-step process; (ii) single step process using bifunctional and hybrid catalysts.

Efficient bifunctional hybrid catalysts, which have a hydrogenation function for the CO_2 hydrogenation to methanol and an acid function for methanol dehydration are required for direct CO_2 hydrogenation into DME. To obtain optimal DME productivity, the catalysts should present a synergy between the hydrogenation and acid functions. Despite the fact that numerous heterogeneous catalysts on the basis of noble metals, metal oxides and chalcogenides have been recently proposed [10, 11] for methanol synthesis from CO_2, Cu-based systems remain the catalytic family *par excellence* for this reaction. Note that copper alone presents low activity for methanol synthesis. The presence of ZnO is usually required. Addition of zinc leads to better copper dispersion, favors [11–14] formation of

Cu^0-ZnO interfaces and Cu-Zn alloys and stabilizes of Cu^+ species. Important, the Cu-ZnO catalysts for methanol synthesis are usually supported on oxide carriers [11, 12, 15]. The oxide carriers affect [14] the catalytic performances by determining texture, exposure of active sites and interaction with reagents, products and reaction intermediates.

No information has been available about the influence of oxide carriers added to the hydrogenation component in the bifunctional catalysts on the direct DME synthesis from CO_2. The goal of this paper is to identify structure-performance correlations in the bifunctional hybrid catalysts prepared using zirconia, alumina and ceria used as oxide carriers for direct synthesis of DME from CO_2 using extended characterization and results of catalytic tests.

2. Experimental

2.1.Synthesis of catalytic materials

The Cu-ZnO-MO_x catalysts with a 60/30/10 wt.% nominal content and being MO_x = Al_2O_3, CeO_2 or ZrO_2 were prepared by co-precipitation. $Cu(NO_3)_2 \cdot 3H_2O$ (Sigma-Aldrich, 99-104%), $Zn(NO_3)_2 \cdot 6H_2O$ (Sigma-Aldrich, ≥ 99%) and $Al(NO_3)_3 \cdot 9H_2O$ (Sigma-Aldrich, ≥ 98%), $Ce(NO_3)_3 \cdot 6H_2O$ (Sigma-Aldrich, 99%) or $ZrO(NO_3)_2 \cdot xH_2O$ (Alfa, 99.9% metal basis) were used as nitrate precursors, while Na_2CO_3 (Acros Organic, 99.5%) was used as precipitating agent. A commercial SAPO-34 zeolite (SiO_2/Al_2O_3 ~0.5, ACS Material) was used as acid catalyst.

Typically, two aqueous solutions containing $Cu(NO_3)_2 \cdot 3H_2O$ (0.38 M) and $Zn(NO_3)_2 \cdot 6H_2O$ (0.19 M) were mixed in a round flask at 70 °C and kept under stirring. Afterwards, a solution containing Al, Ce or Zr nitrates and a 1 M Na_2CO_3 aqueous solution were added dropwise. Then, pH was adjusted to 7 using a 0.1 NaOH aqueous

solution and the mixture was aged for 1 h. The obtained precipitate was then filtered, thoroughly washed with distilled water and dried at 110 °C overnight. The solid was finally calcined at 350 °C for 4 h at a heating rate of 2 °C·min^{-1}. The obtained solids containing Al_2O_3, ZrO_2 or CeO_2 were named CZM, where M= A, Z or C stands for Al, Zr or Ce, respectively.

The hybrid catalytic materials containing the Cu-ZnO-MO_x hydrogenation and SAPO-34 acid components were prepared by mechanical mixture of both solids in an agate mortar. The obtained solids were labelled as CZA//S-34, CZZ//S-34 and CZC//S-34. The typical CZM/S-34 mass ratios were 5 and 1.

2.2.Characterization

The elemental composition of the samples was determined by X-ray fluorescence (XRF). The relative oxide content was determined using a Bruker M4 TORNADO energy dispersive micro-X-ray Fluorescence Spectrometer, equipped with a Rhodium X-ray anode 50 kV/600 mA (30 W) and a Silicon-Drift-Detector Si(Li) with <145 eV resolution at 100000 cps (Mn Kα).

The powder X-ray diffraction (XRD) patterns of the prepared samples were recorded using a Bruker D8 Advance diffractometer. The diffractograms were recorded from 20 to 70° 2θ, using Cu Kα radiation (λ=1.5406 Å) with a step size of 0.01° and a step time of 0.1 s. The determination of the crystallite size was performed using the Scherrer's equation (1):

$$\zeta = K\lambda/\beta\cos\theta \quad (1)$$

where ζ is the crystallite size, K is the shape factor, λ is the X-ray wavelength, β is the corrected line broadening at half-maximum intensity and θ is the Bragg angle at the peak position.

The textural properties of the solids were evaluated by N_2 adsorption-desorption experiments at 77 K. The measurements were carried out using a Micromeritics TriStar II Plus instrument. Prior to the measurements, the samples were degassed for 2 h at 130 °C under vacuum.

The temperature-programmed reduction experiments (H_2-TPR) were carried out using an AutoChem II 2920 V3.05 apparatus (Micromeritics). 20 mg of catalyst were loaded in the reactor and submitted to 50 $mL \cdot min^{-1}$ of H_2 5% v/v in Ar, and the temperature was raised from room temperature (RT) to 900 °C with a heating rate of 10 $°C \cdot min^{-1}$.

The X-ray photoelectron spectroscopy (XPS) measurements were performed using a Kratos Axis Ultra DLD spectrometer using a monochromatized Al X-ray source (1486.6 eV) working at 180 W. The obtained spectra were referenced to the C 1s signal at 284.8 eV, corresponding to adventitious carbon.

The acid properties of the catalysts were evaluated by Ammonia Temperature-Programmed Desorption (NH_3-TPD). The experiments were performed on an Autochem II 2920 V3.05 apparatus (Micromeritics). 1 g of sample was placed in the reactor, reduced under H_2 flow at 350 °C for 1 h and outgassed under He flow. The temperature was afterwards decreased to 100 °C and a series of NH_3 pulses were introduced. Ammonia desorption was monitored by a thermal conductivity detector (TCD) and a mass spectrometer, in the temperature range from 100 to 900 °C.

2.3. Catalytic tests

The catalytic tests of the hybrid catalysts in the direct CO_2 hydrogenation to DME were carried out in a tubular reactor (i. d. 1.4 mm) operating at 10 bar and in the temperature range from 200 to 260 °C. In a typical experiment, 100 mg of the powdered catalyst (125< $Ø_p$ <150 μm) were diluted with SiC to obtain a catalytic bed volume of 0.5 cm^3. Prior to the reaction, the solids were reduced for 1 h at 350°C and atmospheric pressure under 5 $mL \cdot min^{-1}$ of H_2. The pressure was then increased and stabilized, and the flow switched to 5 $mL \cdot min^{-1}$ of the reaction mixture, containing 20% CO_2, 60% H_2 and N_2 as balance. GHSV was 3000 $cm^3\ g_{cat}^{-1}\ h$. The reactants and reaction products were analyzed using an on-line gas chromatography data system (Bruker SCION 456-GC) fitted with ShinCarbon ST and Rt®-Q-BOND columns and TCD and FID detectors. The selectivities to methanol and DME were calculated on carbon basis without considering CO. The details of conversion and selectivity calculations are given in **Supplementary Information (SI)**.

Table 1. Physicochemical properties and composition of the Cu-Zn based CZM and hybrid catalysts (CZM/S-34=5/1)

Catalyst	**S_{BET} ($m^2 \cdot g^{-1}$)**	**CuO (wt.%)**	**ZnO (wt.%)**	**Carrier (wt. %)**
S-34	274.3	-	-	-
CZA	70.9	58.0	25.9	7.6
CZA//S-34	123.1	-	-	-
CZZ	18.8	62.9	23.6	8.0
CZZ//S-34	79.1	-	-	-
CZC	22.2	59.4	31.2	9.5
CZC//S-34	133.5	-	-	-

3. Results and discussion

3.1. Characterization of catalytic materials

The physicochemical properties of the Cu/ZnO based catalysts and hybrid counterparts are shown in **Table 1**. The Cu/ZnO catalysts exhibit specific surface areas ranging from 18.86 to 70.94 $m^2 \cdot g^{-1}$. As expected, addition of the S-34 acid catalyst induces an increase in the specific surface area for all samples. XRF analysis of the CZM methanol catalysts shows a chemical composition of the samples similar to the nominal values.

The XRD patterns of the Cu/ZnO catalysts and S-34 acid catalyst after calcination at 350 °C are presented in **Figure 1**.

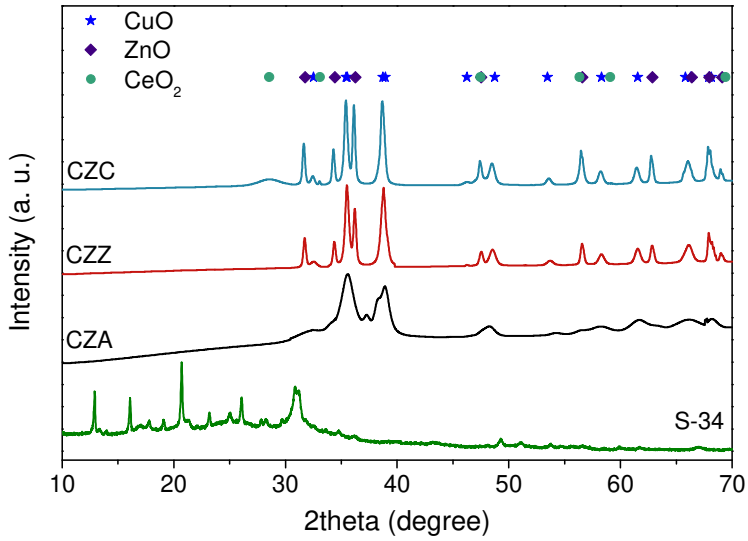

Figure 1. X-ray diffraction patterns of the Cu/ZnO catalysts and the S-34 zeolite after calcination at 350 °C.

The diffractogram of the S-34 acid catalyst presents diffraction peaks typical of a crystalline SAPO-34 zeolite. Regarding the hydrogenation catalysts, CuO (ICDD 00-041-0254) and ZnO (ICDD 00-036-1451) are detected after calcination. In the CZA catalyst, broad peaks of copper and zinc oxides are observed, suggesting the presence of

amorphous or highly dispersed species. On the contrary, intense well-defined diffraction peaks corresponding to CuO and ZnO are detected in the patterns of the ZrO_2 and CeO_2-containing catalysts, thus indicating the presence of crystalline species with larger crystallite sizes. The mean crystallite sizes of CuO and ZnO were calculated using the X-ray line broadening of the (111) and (101) planes respectively, and the results are presented in **Table 2**. Both CuO and ZnO crystallite sizes increase in the order CZA < CZZ < CZC, thus pointing out Al_2O_3 as the oxide carrier allowing higher CuO and ZnO dispersion values. No peaks associated to Al_2O_3 or ZrO_2 are observed in the patterns of the CZA and CZZ catalysts, whereas broad peaks of low intensity corresponding to CeO_2 (ICDD 00-004-0593) are detected in the diffraction patterns of the CZC catalyst, probably due to the low loading of oxide carriers in the samples.

Table 2. CuO and ZnO crystallite sizes, H_2/Cu and H_2/M ratios calculated from TPR profiles and Cu/Cu+Zn atomic ratios for the Cu-ZnO hydrogenation catalysts from XPS.

Catalyst	CuO crystallite size (nm)	ZnO crystallite size (nm)	H_2/Cu ratio [a]	Cu/Cu+Zn before reduction	Cu/Cu+Zn after reduction
CZA	8.5	11.0	0.92	0.53	0.45
CZZ	14.8	30.9	0.98	0.49	0.46
CZC	17.5	63.8	1.00	0.44	0.44

[a] H_2 consumption considered from 200 to 280 °C

The reducibility of the Cu-ZnO catalysts was determined by means of H_2-TPR experiments (**Figure 2**).

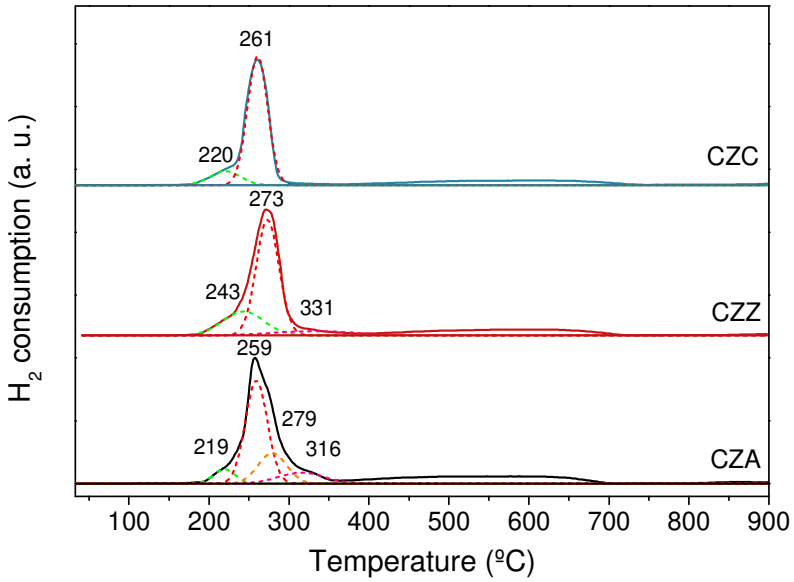

Figure 2. H_2-TPR profiles of the Cu-ZnO based CZM catalysts from RT to 900 °C.

Since the reduction of both ZnO and cerium oxide present in the catalysts may take place at temperatures above 300 °C [16, 17], the TPR peaks in the 200-280 °C temperature range have been attributed to the reduction of Cu^{2+} to Cu^0. After deconvolution of the envelope, every TPR profile presents at least two peaks associated to the reduction of Cu^{2+}, the one at lower temperature is ascribed to the reduction of highly dispersed CuO clusters, followed by the reduction of bulk CuO [18–20]. An additional reduction peak at 279 °C arises in the TPR profile of the CZA catalyst, which has been tentatively attributed to the reduction of Cu^{2+} species included in mixed phases such as $CuAl_2O_4$, whose reduction occurs at higher temperatures than that of pure CuO [18, 20]. The reduction of Cu species takes place at lower temperatures in the CZA and CZC catalysts compared to the CZZ counterpart. Wang [21] *et al.* demonstrated that enhanced reducibility of copper in the methanol synthesis component of the hybrid catalyst significantly improves the DME yield. Accordingly, our H_2-TPR results suggest that DME production could be favored in the catalysts containing Al_2O_3 and CeO_2. The continuous hydrogen consumption between 350 and 700 °C corresponds to the slow reduction of ZnO species

[22], suggesting that after the reduction treatment at 350 °C, a large part of the ZnO species remains oxidized in all catalysts. **Table 2** also shows the H_2/Cu ratios derived from hydrogen consumption in the TPR experiments with the Cu-ZnO CZM catalysts. The value of H_2/Cu is lower than the stoichiometric value for Cu^{2+} reduction (H_2/Cu = 1) for CZA and CZZ.

The valence state of Cu and Zn and the surface composition of the catalysts before and after the reduction treatment at 350 °C was evaluated by XPS. The spectra are presented in **Figure 3.** The relevant information (BE, KE, α') for the assignment of the valence state can be found in **SI, Table S1**.

The Cu 2p XPS spectra of the calcined and reduced catalysts are shown in **Figure 3 (a)**. Due to the overlapping binding energies of Cu^0 and Cu(I), identification of Cu species is not possible through the solely evaluation of the $3p_{1/2}$ and $3p_{3/2}$ core levels, being necessary the examination of their shake-up satellites and the Cu(LMM) spectra [23]. Before reduction, the Cu $2p_{3/2}$ BE values (**SI, Table S1**) in all the catalysts are in good agreement with those reported for CuO, which together with the observed satellite structure confirm the presence of Cu^{2+} species [23, 24]. As reported by Okamoto [25] *et al.*, the satellite intensities relative to the parent peak (I_s/I_p) can give information about the bonding character of Cu^{2+} species. I_s/I_p values in our catalysts are between 0.74 and 0.84, significantly higher than that obtained for pure CuO (~0.55) [25, 26]. This points out the existence of Cu^{2+} species with significantly different from that in CuO in the presence of ZnO, thus suggesting the existence of an interaction between CuO and ZnO, as also suggested by H_2-TPR results.

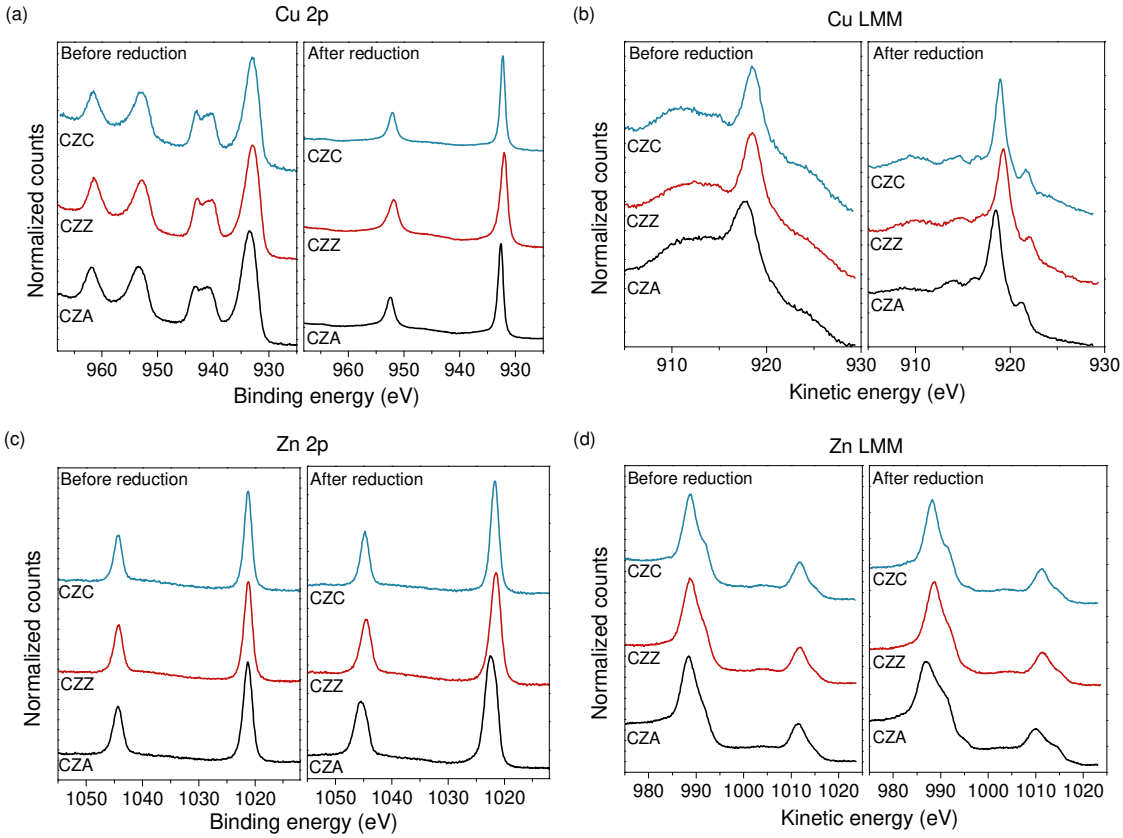

Figure 3. XPS spectra of the Cu-ZnO catalysts before and after reduction under H_2 at 350 °C for 1 h. (a) Cu 2p, (b) Cu LMM, (c) Zn 2p and (d) Zn LMM regions.

The Zn $2p_{3/2}$ BE and Zn(LMM) KE values (**SI, Table S1**) indicate the presence of ZnO in all the catalysts before reduction. However, the Zn LMM spectrum of the CZC sample shows a shoulder at ~991 eV, indicating possible presence of Zn^0 in this catalyst even before the reduction procedure.

After the reduction treatment under H_2 at 350 °C, the shift of the Cu $2p_{3/2}$ peak towards lower BE and disappearance of the Cu 2p satellite peaks characteristic of Cu^{2+} confirm the reduction of Cu^{2+} to lower oxidation states in all the catalysts [24, 27]. Simultaneously, the Cu Auger peak shifts towards higher KE values and a shoulder at

~916.5 eV characteristic of Cu^0 appears [27]. This confirms the total reduction of Cu^{2+} to Cu^0 in all the catalysts as suggested by H_2-TPR results.

The Zn $2p_{3/2}$ peak is shifted to higher BE after the reduction treatment. The Zn LMM region presents a peak at the same BE than before reduction, indicating that a part of the ZnO remains oxidized in all the catalysts after reduction. A shoulder at ~911 eV clearly indicates the partial reduction of ZnO to Zn^0, in good agreement with H_2-TPR results. The Cu/Cu+Zn atomic ratios derived from XPS results were calculated in order to gain insight into Cu species dispersion in the Cu-ZnO catalysts before and after reduction (**Table 2**).

The Cu/Cu+Zn ratio before reduction shows higher Cu species dispersion in the CZA catalyst, followed by CZZ and CZC, in good agreement with the crystallite sizes estimated by XRD. However, this ratio decreases for the CZA and CZZ catalysts after the reduction treatment, indicating some sintering of Cu metal particles during reduction. Furthermore, the treatment under H_2 induces a change in the Cu dispersion trend, being this value slightly higher for CZZ than for CZA. On the contrary, the reduction treatment does not induce Cu dispersion changes in the CZC//S-34 catalyst.

The acidity of the hybrid catalysts was determined by NH_3-TPD. Since the acid sites of comparable strength lead to overlapping peaks, mathematical decomposition is required for separating the contributions [28, 29]. The deconvoluted NH_3-TPD profiles of the S-34 acid catalyst and the hybrid catalysts are presented in **Figure 4**.

Fitting of the NH_3-TPD profiles assuming Gaussian functions shows the existence of three desorption peaks for the S-34 acid catalyst, corresponding to the desorption of NH_3 chemisorbed on weak (< 250 °C), medium (250-400 °C) and strong (> 400 °C) acid sites (**Table 3**) [30, 31]. Total acidity decreases in the hybrid catalysts, although the profiles

shapes obtained are similar to that obtained for the parent acid catalyst. However, a new peak at > 500 °C arises for all the samples, corresponding to the strong acid sites of the Cu-ZnO catalysts [32]. According to previous investigations [33], dehydration of CH_3OH to yield DME is likely to occur in acid sites of weak and moderate strength. Weak acid sites, have been proposed to facilitate methanol dehydration by increasing proton mobility in zeolites [29, 32, 34]. On the contrary, high concentration of strong acid sites should be avoided, since they are known to catalyze undesired reactions yielding hydrocarbons and/or carbon deposits [35].

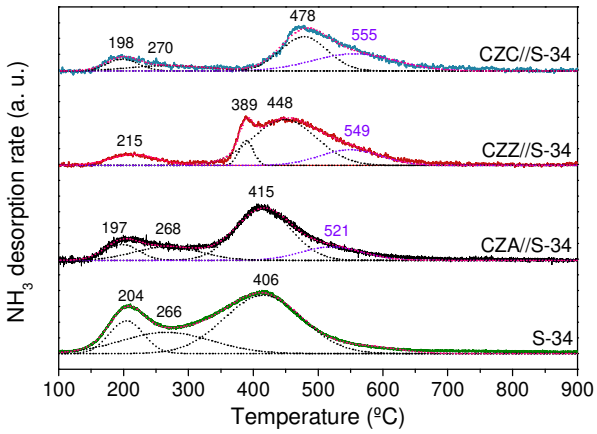

Figure 4. NH_3-TPD profiles of the S-34 acid catalyst and hybrid catalysts (CZM/S-34=5).

In our case, the CZA//S-34 catalyst presents the higher total acidity, followed by CZZ//S-34 and CZC//S-34 (**Table 3**). Interestingly, NH_3 desorption temperatures ascribed to weak and medium acid sites are ~197 °C and ~270 °C for the CZA//S-34 and CZC//S-34 catalysts. On the contrary, higher desorption temperatures of 215 °C and 389 °C are observed for the CZZ//S-34 catalyst. They indicate a higher strength of the weak and medium acid sites in this catalyst and could have an influence on the CH_3OH dehydration step to yield DME.

Table 3. Acid site distribution of the S-34 acid catalyst and hybrid catalysts obtained from NH_3-TPD measurements (CZM/S-34=5)

Catalyst	**Total ($mmol \cdot g^{-1}$)**	**Weak ($mmol \cdot g^{-1}$)**	**Medium ($mmol \cdot g^{-1}$)**	**Strong ($mmol \cdot g^{-1}$)**
S-34	1.39	0.09	0.16	1.14
CZA//S-34	0.17	0.02	0.03	0.12
CZZ//S-34	0.06	0.007	0.005	0.05
CZC//S-34	0.03	0.003	0.003	0.02

3.2.Catalytic performance in the direct synthesis of DME from CO_2

The CO_2 conversion over the hybrid catalysts as a function of the temperature is presented in **Table 4** and **Figure 5**. For all catalysts, CO_2 conversion increases with the temperature. CZA//S-34 is the most active catalyst, followed by CZZ//S-34, which reaches only slightly lower CO_2 conversion values. The duration of the catalytic experiments for each catalyst and at each temperature was at least 20 h. No catalyst deactivation was detected under the reaction conditions.

At 260 °C, both catalysts present similar catalytic performance, reaching the equilibrium conversion. In contrast, the CZC//S-34 catalyst is significantly less active, reaching a maximum CO_2 conversion value of ~9% at 260 °C. This result is consistent with previous observations for the synthesis of methanol from CO_2 [36, 37]. The lower activity of CZC//S-34 has been attributed to lower Cu dispersion induced by the CeO_2 carrier [36], as observed in the CZC//S-34 catalyst by XRD.

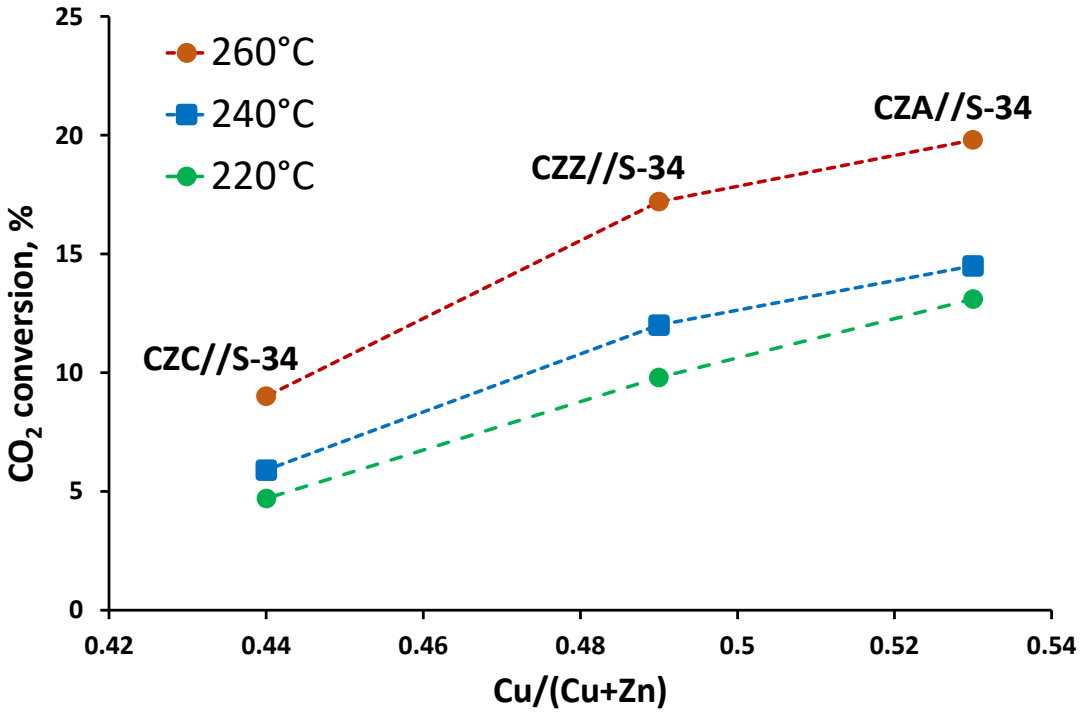

Figure 5. CO_2 conversion over the hybrid catalysts at 220-260 °C as a function of the Cu/Cu+Zn atomic ratio determined by XPS (CZM/S-34=5).

The catalytic activity in the methanol synthesis reaction relies on Cu surface structure. Van den Berg [38] *et al.* demonstrated that the Cu particles smaller than 8 nm gave rise to a drastic decrease in the surface-specific activity, revealing the structure sensitive nature of the reaction. In order to evaluate, whether Cu dispersion also influences the catalytic activity in the synthesis of DME, the CO_2 conversion values in our catalysts have been correlated to the Cu/Cu+Zn ratio calculated by XPS. The results presented in **Figure 5** show a clear the correlation between Cu dispersion and CO_2 conversion values measured at different temperatures. The most active catalyst is that presenting higher Cu dispersion, that is CZZ//S-34, followed by CZA//S-34 and CZC//S-34, thus pointing out the importance of Cu dispersion in the CO_2 hydrogenation.

CO, CH_3OH and DME are the only products detected in all the temperature range. At the reaction pressure of 10 bar, the CO selectivities vary between 51 and 97%, they decrease

to about 50-55 % with the decrease in the reaction temperature to 220°C for CZC//S-34 and CZA//S-34 (**Table 4**). Regardless the oxide carrier, no hydrocarbons formation is observed, being all the catalysts highly selective towards the formation of oxygenated products such as DME and methanol. The CZA//S-34 catalyst presents the best catalytic performance, since the CO_2 conversion value reaches the value determined by thermodynamic equilibrium at 260 °C and selectivity to DME is high, reaching around 55%. Although presenting high CO_2 conversion values in all the temperature range, the CZZ//S-34 catalyst only reaches only 50.9% selectivity to DME. Moreover, the zirconia supported counterpart exhibits extremely high CO selectivity at 260°C. CZA//S-34 has shown the highest single pass DME yield among the studied catalysts (**Table 4**). The CZC//S-34 catalyst also achieves high selectivity towards DME of about 59% even at 260°C, but presents the disadvantage of reaching low CO_2 conversion values compared to their counterparts, which makes it less appropriate for its industrial application in the direct synthesis of DME from CO_2. While strongly affecting the CO selectivity, the reaction temperature does not produce a strong effect of selectivity to methanol and DME.

Table 4. CO_2 conversion and product selectivity over the hybrid catalysts (CZM/S-34=5, P=10 bar, H_2/CO_2=3).

Catalyst	**T**	**X_{CO2}, %**	**S_{CO}, %**	**Selectivity (excluding CO), %**		**DME space yield mmol g_{cat}^{-1} h^{-1}**
				CH_3OH	**DME**	
CZA//S-34	260	19.8	70.9	45.5	54.5	0.78
	240	14.5	73.1	48.0	52.0	0.50
	220	13.1	51.2	48.0	52.0	0.83
CZZ//S-34	260	17.7	97.8	49.0	51.0	0.05
	240	12.0	93.7	45.5	55.4	0.10
	220	9.8	92.2	38.6	61.4	0.12
CZC//S-34	260	9.0	87.9	40.9	59.0	0.16
	240	4.8	80.0	39.1	60.8	0.15
	220	4.7	55.4	39.2	60.5	0.32

Direct DME synthesis from CO_2 requires a carbon dioxide hydrogenation function for methanol synthesis and an acidic function for methanol dehydration [8, 9, 39]. Large amounts of Cu-ZnO sites with a high reducibility and weak acidic sites are needed for hybrid catalysts with satisfactory performance. In addition to kinetics, the direct synthesis of DME from CO_2 has important thermodynamic limitations, especially for the first stage of methanol synthesis. The synergy between the two types of active sites increases [40, 41] the catalytic efficiency of the bifunctional catalyst, which allows the chemical equilibrium to be shifted toward DME and reduces the RWGS reaction yielding CO. In bifunctional catalysis, the entire process thus involves sequential reactions and diffusion of reaction intermediates from one type of site to another.

On the one hand, the two types of active sites in bifunctional catalysts should be [42] as close to each other as possible for higher catalytic activity and better selectivity. On the other hand, very close contact between metal and acid sites often results [43–46] in oxidation and sintering of metallic species, coking and catalyst deactivation. A compromise between enhanced catalytic activity and stability need to be achieved [47]. To ensure good catalyst stability, the hybrid catalysts for direct DME in this work were prepared by mechanically mixing methanol synthesis catalyst and SAPO-34 zeolite catalyst. In a series of catalysts prepared in this work, the best synergy was achieved for CZA//S-34, which exhibited the highest CO_2 conversion rate and less significant CO selectivity.

In order to evaluate the influence of the acid component on the DME synthesis, we varied the ratio of methanol synthesis catalyst and zeolite. A considerable increase in the concentration of acid sites was obtained by decrease in the CZM/S-34 ratio (from 5 to 1) between CO_2 hydrogenation and methanol dehydration components in the hybrid catalysts prepared by mechanical mixing (**SI, Table S2**). Higher concentration of acid

sites and lower amount of hydrogenation sites in the hybrid catalysts affect the CO_2 conversion, but produce a very tiny effect on the DME and methanol selectivities. It also suggests that a relatively small amount of acid sites can be needed for obtaining maximum possible DME selectivity. The step of methanol dehydration into DME can be not kinetically relevant for these catalysts. Indeed, thermodynamic analysis [48] suggests that at 220-260° and P=10 bar, a mixture of methanol and DME will always be present at equilibrium. Higher DME selectivity can be obtained for example, by using a specific operating mode (e.g. DME synthesis from CO_2 combined with water removal [49]). The overall rate of DME synthesis seems to be principally affected by the rate of CO_2 hydrogenation to methanol.

4. Conclusion

A series of Cu-ZnO/MO_x//SAPO-34 hybrid catalysts containing different oxide carriers (MO_x=Al_2O_3, ZrO_2, CeO_2) have been studied for the direct synthesis of DME from CO_2. Copper dispersion was identified as the parameter determining the catalytic performance. Higher copper dispersion was observed in the alumina supported catalysts followed by zirconia and ceria counterparts. The catalysts containing Al_2O_3 and ZrO_2 have shown high catalytic activity, reaching the CO_2 equilibrium conversion at 260 °C. On the contrary, the catalyst containing CeO_2 exhibits a significantly lower catalytic activity, due to significantly lower Cu dispersion. The hybrid catalysts showed variable concentration of weak, medium and strong Bronsted acid sites. The rate of CO_2 hydrogenation seems to be principally affected by the copper dispersion and does not to any large extent depend on the concentration of Bronsted acid sites in the studied catalysts. Under the reaction conditions used in this work, the higher yield of dimethyl ether was observed over the alumina supported copper-zinc catalyst.

Acknowledgements

The authors acknowledge financial support from the European Union ("Electron to Value-Added Chemicals (E2C)" Interreg 2 Seas Project).

References

1. D'Alessandro DM, Smit B, Long JR (2010) Carbon dioxide capture: Prospects for new materials. Angew Chemie - Int Ed 49:6058–6082. https://doi.org/10.1002/anie.201000431

2. Aresta M, Dibenedetto A, Angelini A (2014) Catalysis for the valorization of exhaust carbon: From CO_2 to chemicals, materials, and fuels. technological use of CO_2. Chem Rev 114:1709–1742. https://doi.org/10.1021/cr4002758

3. Ordomsky V V., Dros A-B, Schwiedernoch R, Khodakov AY (2017) Challenges and Role of Catalysis in CO_2 Conversion to Chemicals and Fuels. In: Nanotechnology in Catalysis. Wiley-VCH Verlag GmbH & Co. KGaA, Weinheim, Germany, pp 803–850

4. Ye RP, Ding J, Gong W, et al (2019) CO_2 hydrogenation to high-value products via heterogeneous catalysis. Nat Commun 10:. https://doi.org/10.1038/s41467-019-13638-9

5. Catizzone E, Bonura G, Migliori M, et al (2017) CO_2 Recycling to Dimethyl Ether: State-of-the-Art and Perspectives. Molecules 23:31. https://doi.org/10.3390/molecules23010031

6. Tomatis M, Mahmud Parvez A, Afzal MT, et al (2019) Utilization of CO_2 in renewable DME fuel production: A life cycle analysis (LCA)-based case study in China. Fuel 254:115627. https://doi.org/10.1016/j.fuel.2019.115627

7. Saravanan K, Ham H, Tsubaki N, Bae JW (2017) Recent progress for direct synthesis of dimethyl ether from syngas on the heterogeneous bifunctional hybrid catalysts. Appl Catal B Environ 217:494–522. https://doi.org/10.1016/j.apcatb.2017.05.085

8. Frusteri F, Cordaro M, Cannilla C, Bonura G (2015) Multifunctionality of Cu-ZnO-ZrO_2/H-ZSM5 catalysts for the one-step CO_2-to-DME hydrogenation reaction. Appl Catal B Environ 162:57–65. https://doi.org/10.1016/j.apcatb.2014.06.035

9. Bonura G, Cordaro M, Cannilla C, et al (2014) Catalytic behaviour of a bifunctional system for the one step synthesis of DME by CO_2 hydrogenation. Catal Today 228:51–57. https://doi.org/10.1016/j.cattod.2013.11.017

10. Rodriguez JA, Liu P, Stacchiola DJ, et al (2015) Hydrogenation of CO_2 to Methanol: Importance of Metal-Oxide and Metal-Carbide Interfaces in the Activation of CO_2. ACS Catal 5:6696–6706. https://doi.org/10.1021/acscatal.5b01755

11. Navarro-Jaén S, Virginie M, Bonin J, et al (2021) Highlights and challenges in the selective reduction of carbon dioxide to methanol. Nat Rev Chem 5:564–579. https://doi.org/10.1038/s41570-021-00289-y

12. Arena, F.; Barbera, K.; Italiano, G.; Bonura, G.; Spadaro, L.; Frusteri F (2007) Synthesis, characterization and activity pattern of Cu–ZnO/ZrO_2 catalysts in the

hydrogenation of carbon dioxide to methanol. J Catal 249:185–194. https://doi.org/10.1016/j.jcat.2007.04.003

13. Grandjean D, Pelipenko V, Batyrev ED, et al (2011) Dynamic Cu/Zn Interaction in SiO_2 Supported Methanol Synthesis Catalysts Unraveled by in Situ XAFS. J Phys Chem C 115:20175–20191. https://doi.org/10.1021/jp201839s

14. Arena F, Mezzatesta G, Zafarana G, et al (2013) How oxide carriers control the catalytic functionality of the Cu–ZnO system in the hydrogenation of CO_2 to methanol. Catal Today 210:39–46. https://doi.org/10.1016/j.cattod.2013.02.016

15. Graciani J, Mudiyanselage K, Xu F, et al (2014) Highly active copper-ceria and copper-ceria-titania catalysts for methanol synthesis from CO_2. Science (80-) 345:546–550. https://doi.org/10.1126/science.1253057

16. Liu X-M, Lu GQ, Yan Z-F, Beltramini J (2003) Recent Advances in Catalysts for Methanol Synthesis via Hydrogenation of CO and CO_2. Ind Eng Chem Res 42:6518–6530. https://doi.org/10.1021/ie020979s

17. Shi Z, Xiao X, Mao D, Lu G (2014) Effects of the preparation method on the performance of the $Cu/ZnO/Al_2O_3$ catalyst for the manufacture of l -phenylalaninol with high ee selectivity from l -phenylalanine methyl ester. Catal Sci Technol 4:1132–1143. https://doi.org/10.1039/C3CY00937H

18. Turco M, Bagnasco G, Cammarano C, et al (2007) $Cu/ZnO/Al_2O_3$ catalysts for oxidative steam reforming of methanol: The role of Cu and the dispersing oxide matrix. Appl Catal B Environ 77:46–57. https://doi.org/10.1016/j.apcatb.2007.07.006

19. Arena F, Giovenco R, Torre T, et al (2003) Activity and resistance to leaching of Cu-based catalysts in the wet oxidation of phenol. Appl Catal B Environ 45:51–62. https://doi.org/10.1016/S0926-3373(03)00163-2

20. Velu S, Suzuki K, Okazaki M, et al (2000) Oxidative Steam Reforming of Methanol over CuZnAl(Zr)-Oxide Catalysts for the Selective Production of Hydrogen for Fuel Cells: Catalyst Characterization and Performance Evaluation. J Catal 194:373–384. https://doi.org/10.1006/jcat.2000.2940

21. Wang S, Mao D, Guo X, et al (2009) Dimethyl ether synthesis via CO_2 hydrogenation over $CuO–TiO_2–ZrO_2$/HZSM-5 bifunctional catalysts. Catal Commun 10:1367–1370. https://doi.org/10.1016/j.catcom.2009.02.001

22. Xiao K, Wang Q, Qi X, Zhong L (2017) For Better Industrial $Cu/ZnO/Al_2O_3$ Methanol Synthesis Catalyst: A Compositional Study. Catal Letters 147:1581–1591. https://doi.org/10.1007/s10562-017-2022-8

23. Biesinger MC (2017) Advanced analysis of copper X-ray photoelectron spectra. Surf Interface Anal 49:1325–1334. https://doi.org/10.1002/sia.6239

24. Goodby BE, Pemberton JE (1988) XPS Characterization of a Commercial $Cu/ZnO/Al_2O_3$ Catalyst: Effects of Oxidation, Reduction, and the Steam Reformation of Methanol. Appl Spectrosc 42:754–760. https://doi.org/10.1366/0003702884429148

25. Okamoto Y, Fukino K, Imanaka T, Teranishi S (1983) Surface characterization of copper(II) oxide-zinc oxide methanol-synthesis catalysts by x-ray

photoelectron spectroscopy. 1. Precursor and calcined catalysts. J Phys Chem 87:3740–3747. https://doi.org/10.1021/j100242a034

26. Frost DC, Ishitani A, McDowell CA (1972) X-ray photoelectron spectroscopy of copper compounds. Mol Phys 24:861–877. https://doi.org/10.1080/00268977200101961

27. Okamoto Y, Fukino K, Imanaka T, Teranishi S (1983) Surface characterization of copper(II) oxide-zinc oxide methanol-synthesis catalysts by X-ray photoelectron spectroscopy. 2. Reduced catalysts. J Phys Chem 87:3747–3754. https://doi.org/10.1021/j100242a035

28. Niwa M, Katada N, Sawa M, Murakami Y (1995) Temperature-Programmed Desorption of Ammonia with Readsorption Based on the Derived Theoretical Equation. J Phys Chem 99:8812–8816. https://doi.org/10.1021/j100021a056

29. Rodríguez-González L, Hermes F, Bertmer M, et al (2007) The acid properties of H-ZSM-5 as studied by NH_3-TPD and ^{27}Al-MAS-NMR spectroscopy. Appl Catal A Gen 328:174–182. https://doi.org/10.1016/j.apcata.2007.06.003

30. García-Pérez D, Alvarez-Galvan MC, Campos-Martin JM, Fierro JLG (2021) Influence of the Reduction Temperature and the Nature of the Support on the Performance of Zirconia and Alumina-Supported Pt Catalysts for n-Dodecane Hydroisomerization. Catalysts 11:88. https://doi.org/10.3390/catal11010088

31. Bahruji H, Armstrong RD, Ruiz Esquius J, et al (2018) Hydrogenation of CO_2 to Dimethyl Ether over Brønsted Acidic PdZn Catalysts. Ind Eng Chem Res 57:6821–6829. https://doi.org/10.1021/acs.iecr.8b00230

32. Bonura G, Cordaro M, Spadaro L, et al (2013) Hybrid Cu–ZnO–ZrO_2/H-ZSM5 system for the direct synthesis of DME by CO_2 hydrogenation. Appl Catal B Environ 140–141:16–24. https://doi.org/10.1016/j.apcatb.2013.03.048

33. Yaripour F, Baghaei F, Schmidt I, Perregaard J (2005) Catalytic dehydration of methanol to dimethyl ether (DME) over solid-acid catalysts. Catal Commun 6:147–152. https://doi.org/10.1016/j.catcom.2004.11.012

34. Peinado C, Liuzzi D, Ladera-Gallardo RM, et al (2020) Effects of support and reaction pressure for the synthesis of dimethyl ether over heteropolyacid catalysts. Sci Rep 10:8551. https://doi.org/10.1038/s41598-020-65296-3

35. Mota N, Millán Ordoñez E, Pawelec B, et al (2021) Direct Synthesis of Dimethyl Ether from CO_2: Recent Advances in Bifunctional/Hybrid Catalytic Systems. Catalysts 11:411. https://doi.org/10.3390/catal11040411

36. Angelo L, Kobl K, Tejada LMM, et al (2015) Study of $CuZnMO_x$ oxides (M=Al, Zr, Ce, CeZr) for the catalytic hydrogenation of CO_2 into methanol. Comptes Rendus Chim 18:250–260. https://doi.org/10.1016/j.crci.2015.01.001

37. Zhu J, Ciolca D, Liu L, et al (2021) Flame Synthesis of Cu/ZnO–CeO_2 Catalysts: Synergistic Metal–Support Interactions Promote CH_3OH Selectivity in CO_2 Hydrogenation. ACS Catal 11:4880–4892. https://doi.org/10.1021/acscatal.1c00131

38. van den Berg R, Prieto G, Korpershoek G, et al (2016) Structure sensitivity of Cu and CuZn catalysts relevant to industrial methanol synthesis. Nat Commun

7:13057. https://doi.org/10.1038/ncomms13057

39. Bonura G, Todaro S, Frusteri L, et al (2021) Inside the reaction mechanism of direct CO_2 conversion to DME over zeolite-based hybrid catalysts. Appl Catal B Environ 294:120255. https://doi.org/10.1016/j.apcatb.2021.120255

40. Fan X, Jin B, Ren S, et al (2021) Roles of interaction between components in CZZA / HZSM -5 catalyst for dimethyl ether synthesis via CO_2 hydrogenation. AIChE J 67:. https://doi.org/10.1002/aic.17353

41. Yao L, Shen X, Pan Y, Peng Z (2020) Unravelling Proximity-Driven Synergetic Effect within CIZO–SAPO Bifunctional Catalyst for CO_2 Hydrogenation to DME. Energy & Fuels 34:8635–8643. https://doi.org/10.1021/acs.energyfuels.0c01256

42. Weisz PB (1962) Polyfunctional Heterogeneous Catalysis. Adv. Catal. 13:137-190. https://doi.org/10.1016/S0360-0564(08)60287-4

43. García-Trenco A, Vidal-Moya A, Martínez A (2012) Study of the interaction between components in hybrid CuZnAl/HZSM-5 catalysts and its impact in the syngas-to-DME reaction. Catal Today 179:43–51. https://doi.org/10.1016/j.cattod.2011.06.034

44. Khodakov AY, Ordomsky VV, Palčić A, et al (2020) Assessment of metal sintering in the copper-zeolite hybrid catalyst for direct dimethyl ether synthesis using synchrotron-based X-ray absorption and diffraction. Catal Today 343:199–205. https://doi.org/10.1016/j.cattod.2019.01.023

45. Ordomsky VV, Cai M, Sushkevich V, et al (2014) The role of external acid sites of ZSM-5 in deactivation of hybrid CuZnAl/ZSM-5 catalyst for direct dimethyl ether synthesis from syngas. Appl Catal A Gen 486:266–275. https://doi.org/10.1016/j.apcata.2014.08.030

46. Cai M, Palčić A, Subramanian V, et al (2016) Direct dimethyl ether synthesis from syngas on copper–zeolite hybrid catalysts with a wide range of zeolite particle sizes. J Catal 338:227–238. https://doi.org/10.1016/j.jcat.2016.02.025

47. Bonura G, Todaro S, Frusteri L, et al (2021) Inside the reaction mechanism of direct CO_2 conversion to DME over zeolite-based hybrid catalysts. Appl Catal B Environ 294:120255. https://doi.org/10.1016/j.apcatb.2021.120255

48. Stangeland K, Li H, Yu Z (2018) Thermodynamic Analysis of Chemical and Phase Equilibria in CO_2 Hydrogenation to Methanol, Dimethyl Ether, and Higher Alcohols. Ind Eng Chem Res 57:4081–4094. https://doi.org/10.1021/acs.iecr.7b04866

49. van Kampen J, Boon J, Vente J, van Sint Annaland M (2020) Sorption enhanced dimethyl ether synthesis for high efficiency carbon conversion: Modelling and cycle design. J CO2 Util 37:295–308. https://doi.org/10.1016/j.jcou.2019.12.021